Network pharmacology combined with experimental validation to investigate the effect of Rongjin Niantong Fang on chondrocyte apoptosis in knee osteoarthritis

JUN CHEN[1,2*], TING ZHANG[1*], QINGQING LUO[2*], RUYI WANG[1*], YUTING DAI[2], ZHENYUAN CHEN[2], CHUTIAN ZHANG[3], XUZHENG CHEN[3] and GUANGWEN WU[1,2]

[1]School of Traditional Chinese Medicine, Fujian University of Traditional Chinese Medicine; [2]Key Laboratory of Orthopedics and Traumatology of Traditional Chinese Medicine and Rehabilitation (Fujian University of Traditional Chinese Medicine), Ministry of Education; [3]Academy of Integrative Medicine, Fujian University of Traditional Chinese Medicine, Fuzhou, Fujian 350122, P.R. China

Received November 15, 2023; Accepted February 27, 2024

DOI: 10.3892/mmr.2024.13226

Abstract. Knee osteoarthritis (KOA) is a chronic degenerative disease that affects the quality of life of middle-aged and elderly individuals, and is one of the major factors leading to disability. Rongjin Niantong Fang (RJNTF) can alleviate the clinical symptoms of patients with KOA, but the molecular mechanism underlying its beneficial effects on KOA remains unknown. Using pharmacological analysis and *in vitro* experiments, the active components of RJNTF were analyzed to explore their potential therapeutic targets and mechanisms in KOA. The potential targets and core signaling pathways by which RJNTF exerts its effects on KOA were obtained from databases such as Gene Expression Omnibus, Traditional Chinese Medicine Systems Pharmacology and Analysis Platform. Subsequently, chondrocyte apoptosis was modeled using hydrogen peroxide (H_2O_2). Cell Counting Kit-8 assay involving a poly [ADP-ribose] polymerase-1 (PARP1) inhibitor, DAPI staining, reverse transcription-quantitative PCR, Annexin V-FITC/PI staining and flow cytometry, western blotting and co-immunoprecipitation analysis were used to determine the therapeutic efficacy of RJNTF on KOA and to uncover the molecular mechanism. It was found that PARP1-knockdown lentivirus, incubation with PARP1 inhibitor PJ34, medium and high doses of RJNTF significantly reduced H_2O_2-induced chondrocyte apoptosis. Medium and high doses of RJNTF downregulated the expression of cleaved caspase-3, cleaved PARP1 and PAR total proteins, as well as nucleus proteins of apoptosis-inducing factor (AIF) and migration inhibitory factor (MIF), and upregulated the expression of caspase-3, PARP1 total protein, as well as the cytoplasmic expression of AIF and MIF, suggesting that RJNTF may inhibit chondrocyte apoptosis through the PARP1/AIF signaling pathway.

Correspondence to: Professor Guangwen Wu, School of Traditional Chinese Medicine, Fujian University of Traditional Chinese Medicine, 1 Qiuyang Road, Fuzhou, Fujian 350122, P.R. China
E-mail: wuguangwenfj@163.com

*Contributed equally

Key words: knee osteoarthritis, Rongjin Niantong Fang, PARP1/AIF pathway, apoptosis, network pharmacology

Introduction

Knee osteoarthritis (KOA) is a common disease affecting the quality of life of middle-aged and elderly individuals (1). With an ever-aging society, the incidence of KOA is increasing annually (2). Clinical manifestations include joint pain, swelling, limited movement and joint friction, and the end stage of the disease can result in disability (3). The cause of KOA is primarily related to sex, age, obesity, heredity factors, mechanical force and congenital joint anomalies amongst other factors. KOA is the result of a normal coupling imbalance between the degradation and synthesis of chondrocytes, extracellular matrix and cartilage. It is caused by a combination of mechanical and biological factors leading to an imbalance in the normal coupling of degradation and synthesis of the subchondral bone, and the degeneration of articular cartilage is the characteristic and basic pathological change of KOA (4-6).

Chondrocytes, the core components of cartilage tissue, have the function of maintaining the normal structure and the physiology of cartilage. When the number of chondrocytes decreases, for example due to autophagy, senescence and apoptosis, the structure and the function of the cartilage are affected (7-10). Poly [ADP-ribose] polymerase-1 (PARP-1)-dependent cell death, known as parthanatos, (11-13) is caused by the overactivation of PARP1, which catalyzes the catabolism of intracellular nicotinamide adenine dinucleotide (NAD) to produce poly [ADP-ribose] (PAR), which is translocated to the cytoplasm and binds to the outer surface of the mitochondria, causing the release of apoptosis-inducing factor (AIF) and the recruitment of macrophage migration inhibitory factor (MIF) to the nucleus, where it acts as a DNA

endonuclease in synergy with nucleic acid exonuclease G to induce chromatin condensation and DNA breaks, generating fragments ~50 kb in length and inducing apoptosis in parthanatos (12,14,15). No research has revealed the association of PARP1/AIF with chondrocyte apoptosis.

Rongjin Niantong Fang (RJNTF) originates from 'Qing Gong Pei Fang Ji Cheng' which was compiled by the academic Chen Keji, and consists of six component herbs, *Achyranthes bidentata* Blume (Niu Xi), *Angelica sinensis* (Oliv) Diels (Dang Gui), *Heracleum hemsleyanum* Diels (Du Huo), *Hansenia weberbaueriana* (Fedde ex H. Wolff) Pime (Qiang Huo), *Saposhnikovia divaricata* (Turcz.) Schischk (Fang Feng) and *Glycyrrhiza uralensis* Fisch (Gan Cao). As a well-known Traditional Chinese folk medicine, it is used to invigorate the circulation of swelling, relieve pain caused by arthralgia pain, nourish the liver and kidney, and promote blood circulation; it is commonly used for the treatment of various diseases, including KOA (16). It is known that certain active ingredients of RJNTF are known to act directly on chondrocytes (17,18), but its mechanism of action has not yet been thoroughly investigated and explained. The aim of the present study was to provide a scientific basis for the application of RJNTF in the treatment of KOA. It is unknown whether RJNTF can inhibit chondrocyte apoptosis by regulating the PARP1/AIF signaling pathway. To further clarify the mechanism of action of this drug and assess its potential as a treatment for KOA, the current study investigated the inhibition of chondrocyte apoptosis by RJNTF through modulation of the PARP1/AIF pathway using web-based pharmacological analytical tools and *in vitro* experiments. Finally, the findings of the present study revealed that inhibition of PARP1 can effectively suppress chondrocyte apoptosis, provide new insights and understanding of the mechanism of action of folk medicine, help to promote the clinical translation of folk medicine in the treatment of KOA and provide important references for further research and clinical practice.

Materials and methods

Network pharmacology analysis. The data of normal human cartilage and KOA cartilage were retrieved and downloaded from the Gene Expression Omnibus database (accession no. GSE75181) (19), and the merged gene expression matrix was analyzed using the limma package in R (version 4.0.5) and R Studio (version 4.0.5) (20-22) to screen the differentially expressed genes (DEGs). The DEGs of KOA were obtained by screening using the criteria |log2 (fold change)| ≥1 and P_{adj}<0.05, and a volcano map was plotted using Hiplot Pro (BGI Group; https://hiplot.com.cn/). The Traditional Chinese Medicine Systems Pharmacology (TCMSP) database (https://old.tcmsp-e.com/tcmsp.php) was used to identify the active ingredients of RJNTF, and then the Search Tool for Interacting Chemicals (http://stitch.embl.de/) database was used to retrieve the potential targets of each active ingredient. Venn diagrams were used to visualize the overlapping targets of RJNTF with the DEGs of KOA. Protein-protein interaction (PPI) analysis was used in the BisoGenet plug-in of Cytoscape software (version 3.8.2) (23), and the results were analyzed based on the topological parameters using the CytoNCA plug-in (http://apps.cytoscape.org/apps/cytonca) to obtain the key targets of RJNTF (24). Kyoto Encyclopedia of Genes and Genomes (KEGG) pathway enrichment analysis was performed on the potential targets of RJNTF that were common DEGs of KOA using the clusterProfiler package in R (version 4.0.5); the potential targets related to apoptosis signaling pathways were obtained, and the key target-signaling pathway map was constructed using Cytoscape (25,26).

Primary reagents and antibodies. RJNTF is comprised of *Achyranthes bidentata*, *Angelica sinensis*, *Angelica biserrata*, *Hansenia weberbaueriana*, *Saposhnikovia divaricata* and *Glycyrrhiza uralensis* at a ratio of 4:2:3:2:2:2. The decoction protocol of RJNTF included adding water at a solid:liquid ratio of 1:10, decocting three times for 1.5 h each time, then filtering the liquid each time to remove the dregs, before combining and mixing, evaporation of the mixed liquid to lyophilize into powder, and storing the lyophilized powder in a vacuum drying oven (preparation method and use of formula authorized by the National Invention Patent; patent nos. ZL201710284659.8 and ZL201810899834.9) (27). The Cell Counting Kit-8 (CCK-8) reagent was purchased from MedChemExpress. DAPI was purchased from Beijing Solarbio Science & Technology Co., Ltd. The Novolink™ Polymer Detection System was purchased from Fuzhou Maixin Biotech Co., Ltd. The Annexin V-FITC Apoptosis Detection Kit was purchased from Nanjing KeyGen Biotech Co., Ltd. L-DMEM was purchased from Shanghai BasalMedia Technologies Co., Ltd. Hydrogen peroxide (H_2O_2) and FBS were purchased from MilliporeSigma. PARP1-knockdown lentiviral vector was constructed by Shanghai GeneChem Co., Ltd. The PCR primers and the Nuclear and Cytoplasmic Protein Extraction Kit used were obtained from Shanghai Biotechnology Co., Ltd. The PARP1 inhibitor PJ34 was purchased from MedChemExpress.

Separation and culture of articular chondrocytes. A total of 30 Male Sprague-Dawley (SD) rats (4-week-old; 80±10 g) were purchased from SLAC Laboratory Animal Technology Co., Ltd. [animal license no. SCXK (Hu) 2019-0007] and were used to obtain chondrocytes from the knee articular cartilage, which is relatively easy to obtain. The chondrocytes of 4-week-old rats are in active growth and development, their metabolism is active and the number of chondrocytes is large so they can better adapt to the *in vitro* culture environment (28,29). Tissues were collected in accordance with the Animal Care and Use Committee of Fujian University of Traditional Chinese Medicine (IACUC issue no. FJTCM IACUC 2022044) and the Declaration of Helsinki. The 4-week-old SPF-grade SD male rats were euthanized by intraperitoneal injection with 100 mg/kg pentobarbital sodium. The cessation of breathing and heart rate were used to confirm the death of the rats. The cartilage of the knee joints was obtained under aseptic conditions. The cartilage was rinsed with PBS three times, and then cut into 1x1x1-mm pieces with a scalpel blade, cleaned with PBS again, and transferred to a 60-mm culture dish; 5 ml 0.2% type II collagenase solution containing 1% penicillin, streptomycin and amphotericin B triple antibiotic solution, which was purchased from Shanghai BasalMedia Technologies Co., Ltd., and placed in a cell culture incubator at 5% CO_2 and 37˚C for digestion, collecting the cells every 2 h. The supernatant was aspirated using a pipette and filtered through a 200-mesh nylon

sieve. The filtrate was transferred to a 15-ml Eppendorf tube, centrifuged at 1,000 x g for 3 min at room temperature, and the supernatant was discarded; 4 ml complete medium was used to resuspend the cell pellet, and then cultured uniformly in T25 cell culture flasks and incubated for chondrocyte cell culture. Digestion was carried out by adding 5 ml 0.2% collagenase solution containing 1% antibiotic to the original 60-mm petri dish for a total of three times. After 24 h, the culture medium was replaced when the cells had adhered, and the medium was changed every 2 days. Cell growth was observed using an inverted light microscope. When the cell confluence reached ~90%, the chondrocytes were subcultured with 2.5 g/l trypsin (Promega Corporation) and 0.02% EDTA. Chondrocytes at passage two were used for subsequent experiments.

Cell viability assay. According to the manufacturer's instructions, a CCK-8 kit was used to separately evaluate the effects of the different concentrations of H_2O_2, PJ34 and RJNTF on the viability of the chondrocytes. Second-generation chondrocytes were seeded in 96-well plates (2,000 cells/well), and then exposed to H_2O_2 for 4 h (0, 100, 200, 300, 400, 500, 600, 700 or 1,000 μM), PJ34 for 4.5 h (0.001, 0.01, 0.1, 1, 10, 100 or 1,000 μM), and RJNTF (0, 100, 200, 400, 800, 1,600, 3,200, 6,400 or 12,800 μg/ml) for 24, 48 or 72 h, respectively. Each well was treated with 10% CCK-8 solution and incubated for further 2 h at 37˚C. The absorbance was detected at 450 nm using an EnSpire® multimode plate reader (PerkinElmer, Inc.).

DAPI staining. Chondrocytes ($2x10^5$ cells/well) were seeded into cell crawls placed in 6-well plates. After 24 h of incubation, the cell crawls were transferred into a new 6-well plate and washed twice with PBS. After fixation with 4% Paraformaldehyde Fix Solution (Beyotime Institute of Biotechnology) for 30 min and rinsing twice with PBS, the chondrocytes were stained with 500 μl DAPI for 10 min at room temperature and then washed twice with PBS for a total of 3 min per wash. The cellular morphology was observed under a Leica DMi8 inverted fluorescence microscope (Leica Microsystems, Inc.).

Flow cytometry. The Annexin V-FITC/PI apoptosis kit was used according to the manufacturer's protocol. Briefly, chondrocytes were collected and rinsed twice with PBS. Next, chondrocytes were labeled with 500 μl 1x binding buffer with 5 μl PI and 5 μl Annexin V-FITC for 15 min in the dark. Apoptosis rates were measured using a Cyto FLEX flow cytometer (Beckman Coulter Inc.) and CytExpert (version 2.4; Beckman Coulter, Inc.).

Knockdown of PARP1. Chondrocytes ($2x10^5$ cells/well) were seeded into 96-well plates. A short interfering RNA (si)-negative control (NC), si-PARP1 #1 (positive virus 114447), si-PARP1 #2 (positive virus 114448) and si-PARP1 #3 (positive virus 114449) with green fluorescent protein were purchased from GeneChem, Inc. (Table I). After 24 h, the viruses were stored at -80˚C and taken out when required, placing on ice to thaw. The four viruses were individually diluted to an multiplicity of infection (MOI) of 100, 50 and 10 using complete medium. The culture media was discarded from cells, and using Nucleic acid transfection kit (Shanghai Genechem, Inc.) with nucleic acid concentration at $1x10^8$ TU/ml and the effective transfection enhancers HiTransG A and HiTransG P (GeneChem, Inc.) were added according to the grouping, and mixed and cultured at 37˚C, with 5% CO_2, for 16 h. After transfection, the medium was replaced with 10% FBS DMEM, and cells were incubated at 37˚C, with 5% CO_2 for 48 h, and the transfection efficiency was evaluated under a fluorescence microscope. The transfection efficiency was calculated as follows: Transfection efficiency=(number of fluorescent cells/total number of cells) x100. After singling out viruses with high transfection efficiency, the chondrocyte apoptosis model was replicated.

Table I. Sequences of si-PARP1s and si-NC.

Gene	Sequences (5'-3')
PARP1-RNAi(114447)	GCTGATCTGGAATATCAAAGA
PARP1-RNAi(114448)	GGAGGCAAGTTGACAGGATCT
PARP1-RNAi(114449)	GCACAGTTATCGGCAGTAACA
si-NC	TTCTCCGAACGTGTCACGT

PARP1, poly [ADP-ribose] polymerase-1; si-NC, short interfering RNA-negative control; RNAi, RNA interference.

Reverse transcription-quantitative PCR (RT-qPCR). Chondrocytes ($3x10^6$ cells/well) were seeded in 6-well plates and treated with one of the aforementioned different siRNA constructs. Total RNA was extracted from cells using TRIzol® reagent (Invitrogen; Thermo Fisher Scientific, Inc.) and the RNA concentration was measured. cDNA was synthesized using an Evo M-MLV RT kit (Hunan Acre Bioengineering Co., Ltd.), according to the manufacturer's protocol, and amplified by qPCR using SYBR Green Pro Tap (Hunan Acre Bioengineering Co., Ltd.) on a Bio-Rad CFX96 amplifier. The thermocycling conditions were 95˚C for 3 min; followed by 40 cycles of amplification at 95˚C for 10 sec and 60˚C for 30 sec. β-actin was used as the internal control, and relative gene expression was normalized to β-actin mRNA expression and analyzed using the $2^{-\Delta\Delta Cq}$ method (30). The sequences of the primers are listed in Table II.

Western blotting. Cells were washed three times with cold PBS and blotted dry, and then 120 μl RIPA (Beyotime Institute of Biotechnology) buffer supplemented with 1 mM PMSF was added for 30 min on ice; the petri dish was shaken once every 10 min, and the lysate was transferred to a 1.5 ml EP tube which was centrifuged at 4˚C for 5 min at 12,000 x g. The supernatant was collected, and a total of 5 μl supernatant was used for BCA protein quantification, and 5x SDS-PAGE protein sampling buffer was added to the remaining supernatant. Nucleus and cytoplasmic proteins were extracted according to the manufacturer's instructions using Nuclear and Cytoplasmic Protein Extraction Kit (Beyotime Institute of Biotechnology; cat. no. P0028), and the buffer was mixed with the protein supernatant and then heated in a thermostatic metal bath at 99˚C for 10 min to denature the proteins sufficiently and stored at -80˚C. A total of 30 μg protein sample was loaded per lane and separated by 10% or 15% SDS-PAGE at 30 V for 10 min, 80 V

Table II. Primer sequences used in reverse transcription-quantitative PCR.

Gene	Forward primer (5'-3')	Reverse primer (5'-3')
PARP1	CTTGGTGGAGTACGAGATTGAC	GGTGTAGAAGCGATTGGAGAG
β-actin	TCACCCACACTGTGCCCATCTATGA	CATCGGAACCGCTCATTGCCGATAG

PARP1, poly [ADP-ribose] polymerase-1.

for 30 min, and 110 V for 55 min and subsequently transferred to a 0.45-μm PVDF membrane; 15% PAGE gels were used for caspase-3, cleaved-caspase-3, AIF, MIF, histone and β-actin, while 10% PAGE gels were used for PARP1, cleaved-PARP1, PAR and β-actin. Both the target protein and the corresponding internal reference were run on the same membrane; this was cut into strips and each was probed separately to ensure that every protein can be incubated with a specific antibody. After the membranes were blocked with NcmBlot blocking buffer for 10 min at 25˚C, membranes were incubated with primary antibodies against PARP1 (1:5,000; Proteintech Group, Inc.; cat. no. 66520-1-Ig), caspase-3 (1:1,000; Proteintech Group, Inc.; cat. no. 19677-1AP), cleaved PARP1 (1:1,000; Cell Signaling Technology, Inc.; cat. no. 94885S), cleaved caspase-3 (1:1,000; Cell Signaling Technology, Inc.; cat. no. 9661S), PAR (1:200; Enzo Life Sciences, Inc.; cat. no. ALX-804-220-R100), AIF (1:1,000; cat. no. 5318S; Cell Signaling Technology, Inc.), MIF (1:1,000; Abcam; cat. no. Ab175189), β-actin (1:1,000; Cell Signaling Technology, Inc.; cat. no. 8457S), or histone (1:1,000; Abcam; cat. no. Ab1791) at 4˚C overnight. The following day, membranes were washed with TBST (TBS with 0.1% Tween-20, 10X) three times and subsequently incubated with corresponding the HRP-conjugated secondary antibodies (1:20,000; Cell Signaling Technology, Inc.; cat. no. 7074S) at 25˚C for 1 h. The membranes were rinsed three times with TBST, and signals were visualized with a Bio-Rad ChemiDoc MP Imaging System (Bio-Rad Laboratories, Inc.), which using enhanced chemiluminescence western blot substrate. Densitometry analysis was performed using ImageJ (version win64; National Institutes of Health) and normalized to the respective β-actin or histone band.

Co-immunoprecipitation (IP) assay. Diluted antibody (400 μl) against AIF (1:1,000; cat. no. 5318S; Cell Signaling Technology, Inc.), MIF (1:1,000; cat. no. Ab175189; Abcam) and β-actin (1:1,000; cat. no. 8457S; Cell Signaling Technology, Inc.) was aspirated into 50 μl magnetic beads and mixed well, before incubation at 4˚C for 2 h. After magnetic separation, the magnetic beads were collected, 500 μl phosphate-buffered saline (Shanghai BasalMedia Technologies Co., Ltd.) was added, the magnetic beads were mixed well and the supernatant was discarded after magnetic separation. Washing was performed four times. A total of 200 μl lysis buffer (Beyotime Institute of Biotechnology) was added, followed by lysis at 4˚C for 30 min, with agitation of the cells every 10 min to ensure full contact with the lysis buffer, and then centrifugation at 4˚C for 10 min at 12,000 x g. The supernatant was collected and set aside at 4˚C. After BCA quantification, 20 μl SDS-PAGE loading buffer was added to the magnetic beads and mixed uniformly, after which the magnetic beads were heated at 99˚C for 10 min, the beads were separated and the supernatant was used for western blotting.

Statistical analysis. Data analysis was performed using GraphPad Prism (version 8.0; Dotmatics). A unpaired two-sample t-test was used to compare differences between two groups. For multiple group comparisons, one-way ANOVA was used, followed by Tukey's post hoc test. $P<0.05$ was considered to indicate a statistically significant difference.

Results

Network pharmacology analysis to determine the key targets and core signaling pathways in the treatment of KOA with RJNTF

Differential genes of KOA and key targets of RJNTF. A total of 644 significantly altered and affected differential genes were obtained including 423 upregulated genes and 221 downregulated genes (Fig. 1A). A total of 45 active ingredients of RJNTF were obtained by screening using the TCMSP database, corresponding to 234 targets. There were 29 common targets between KOA and RJNTF as shown by the Venn diagram in Fig. 1B; the number of active ingredients corresponding to each drug was 6 for *Achyranthes bidentata* Blume, 10 for *Glycyrrhiza uralensis* Fisch, 4 for *Hansenia weberbaueriana* (Fedde ex H. Wolff) Pime, 3 for *Heracleum hemsleyanum* Diels, 11 for *Saposhnikovia divaricata* (Turcz.) Schischk and 11 for *Angelica sinensis* (Oliv) Diels (Fig. 1C).

Key targets of RJNTF for the treatment of KOA. The targets of RJNTF for the treatment of KOA were imported into Cytoscape to generate the PPI network, and a total of 1,966 related targets and 48,840 target-to-target interrelationships were obtained; the plugin CytoNCA was further used to filter the network nodes based on their topological attributes using the degree centrality value, after which, 531 relevant targets and 2,218 target-target interrelationships were obtained by excluding irrelevant nodes. Finally, 143 key targets and 3,600 target-target interrelationships were obtained by screening with the betweeness centrality value, including STAT3, PI3K, RAF, RAS, AKT, PARP1 and JALK2, the mechanisms of which include proliferation, inflammation and apoptosis. After layers of screening, PARP1, a special apoptosis target, was found among several targets (Fig. 2A).

Core signaling pathway of RJNTF in treating KOA. The results of KEGG analysis showed that RJNTF could treat KOA by interfering with multiple signaling pathways such as NF-κB,

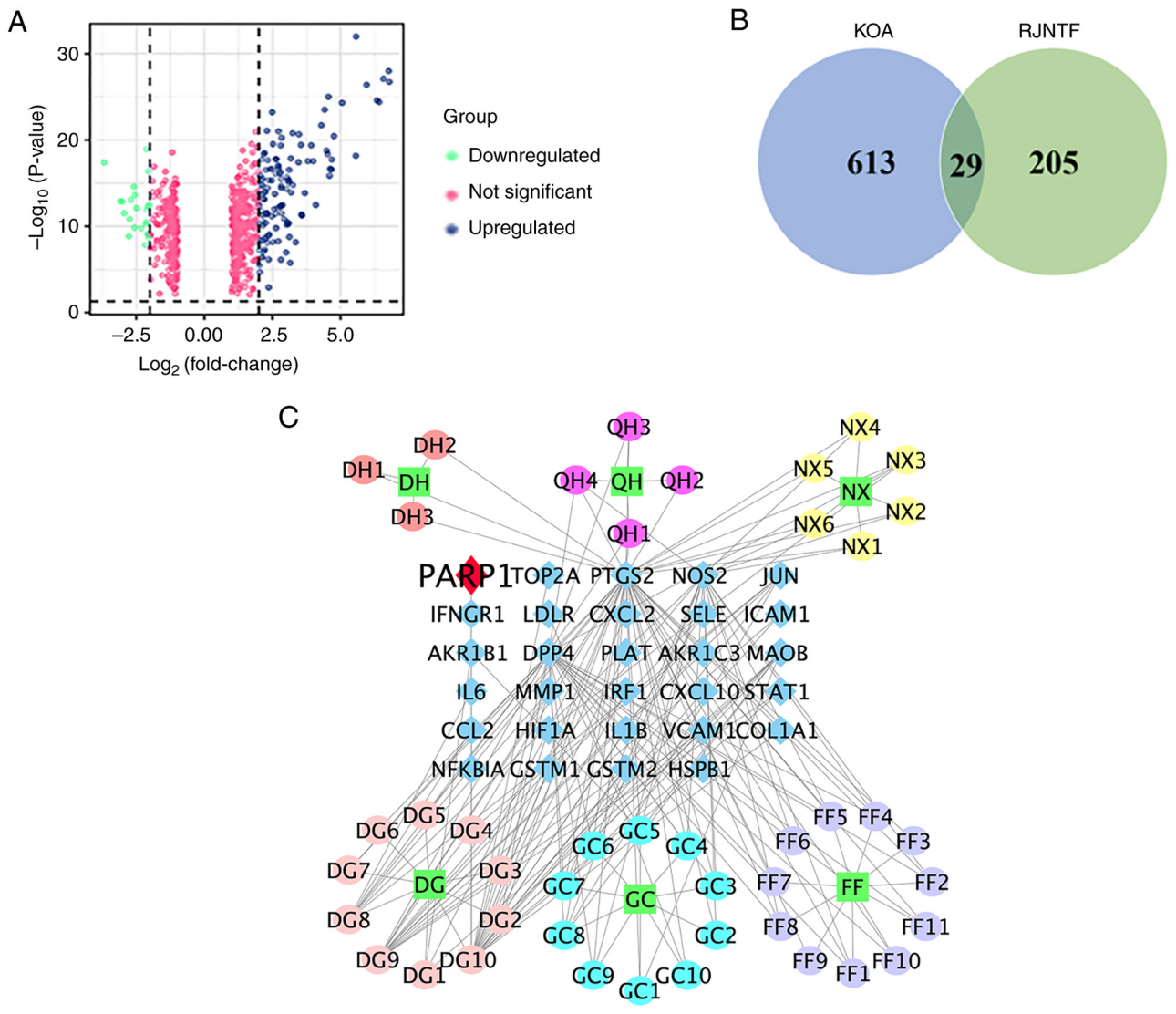

Figure 1. Identification of targets common to both RJNTF and KOA. (A) Volcano plot of the differentially expressed genes in OA. Sample data of the knee joints of patients with OA from the Gene Expression Omnibus database. Green represents downregulated genes, blue represents upregulated genes, and pink represents no significant change. (B) Venn diagram of the genes common to both KOA and RJNTF. (C) Active ingredients and key targets of RJNTF. Green squares represent the drug, blue diamonds represent genes, and circles represent the active ingredient of the drug; the darker red color represents DH, the rosy red color represents the active ingredient of QH, the yellow color represents NX, the pink color represents DG, the azure color represents GC and the purple color represents FF; RJNTF, Rongjin Niantong Fang; KOA, knee osteoarthritis; PARP1, poly [ADP-ribose] polymerase-1; DH, *Heracleum hemsleyanum* Diels; QH, *Hansenia weberbaueriana* (Fedde ex H. Wolff) Pime; NX, *Achyranthes bidentata* Blume; DG, *Angelica sinensis* (Oliv) Diels; GC, *Glycyrrhiza uralensis Fisch;* FF, *Saposhnikovia divaricata* (Turcz.) Schischk.

apoptosis, HIF-1 signaling pathway, JAT-STAT signaling pathway and IL-17 signaling pathway (Fig. 2B) (31-34). Based on the results of a large number of previous studies showing that the PARP1/AIF pathway was closely related to apoptosis (35-37), while the results of network pharmacology indicated that the treatment of KOA by RJNTF was related to the PARP1 apoptotic pathway; however, there are no studies assessing the relationship between the PARP1/AIF pathway and apoptosis of chondrocytes. Therefore, the subsequent experiments were designed to ascertain the underlying mechanism.

Inhibition of chondrocyte apoptosis through modulation of the PARP1/AIF pathway

Establishment and characterization of an apoptotic articular chondrocyte cell model. Characterization of normal chondrocytes is shown in Fig. 3A. In the process of chondrocyte culture, observed by inverted phase contrast optical microscope, after 1 day, chondrocytes were completely attached to the wall and began to divide and grow, and most of the cells were round or oval. After 7 days of culture, the number of chondrocytes were markedly increased, and grew in clusters in the shape of pavements; clusters were connected with each other in a long piece, and the speed of proliferation was accelerated. When the cells were grown up to 80% of the density, they could be subcultured to obtain the F1 chondrocytes. After 3 days of culture, the cytoplasm was abundant, the nuclei were clearly distinguishable and the edges of the cells were sharp. After ~4 days of culture, F2 cells could be obtained by substitution; F2 cells at this time could still maintain a better morphology, with no obvious tendency of hypertrophy and degradation, whereas F3 cells appeared to have more hypertrophic and

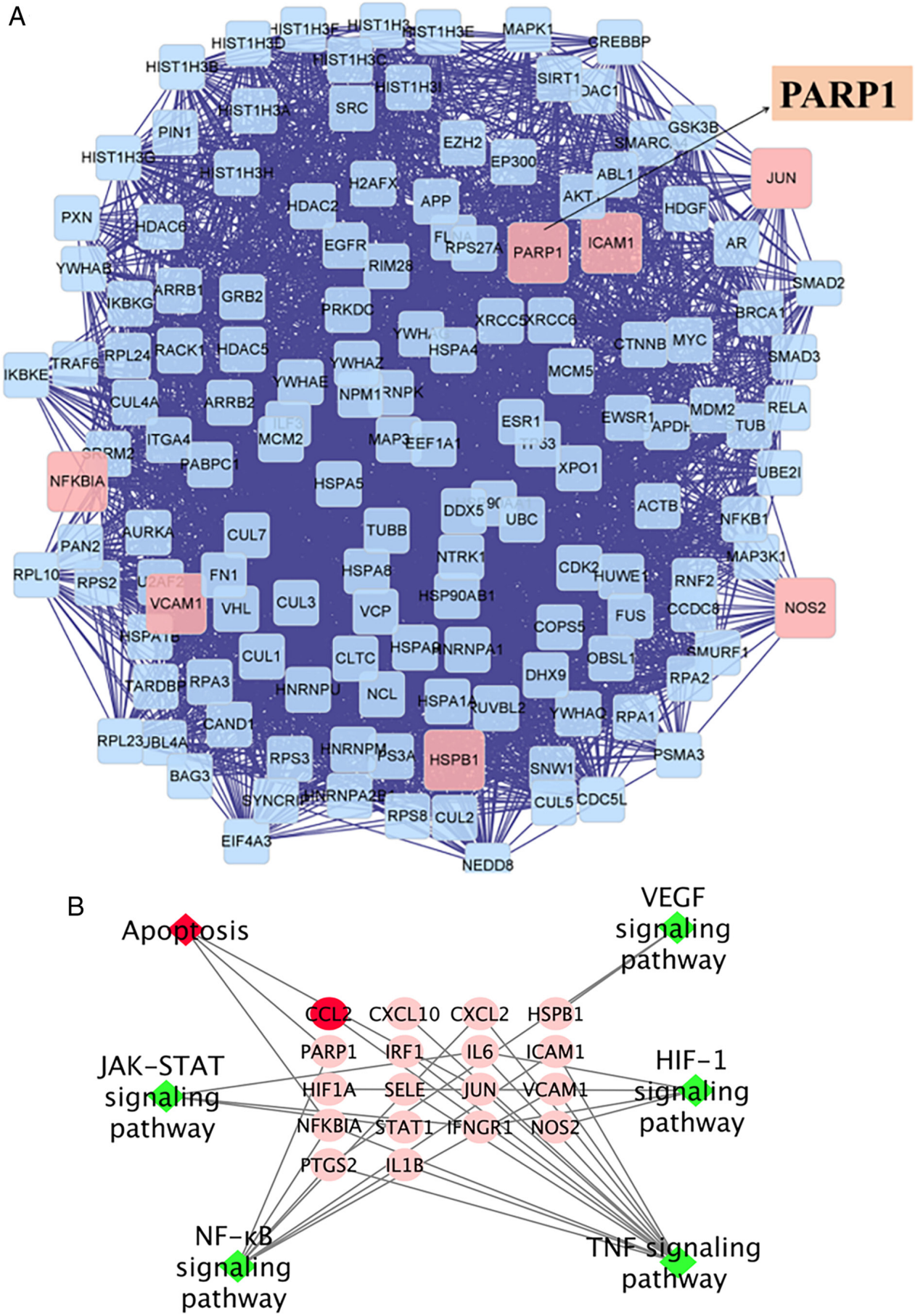

Figure 2. Network pharmacological analysis of chondrocyte apoptosis modulation by RJNTF. (A) Process of topological screening and protein interactions for the PPI network. (B) Target-signaling pathway diagram of RJNTF. Pink circles represent targets and green diamonds represent pathways; apoptotic targets and pathways are highlighted in dark red. RJNTF, Rongjin Niantong Fang; PPI, protein-protein interaction; PARP1, poly [ADP-ribose] polymerase-1.

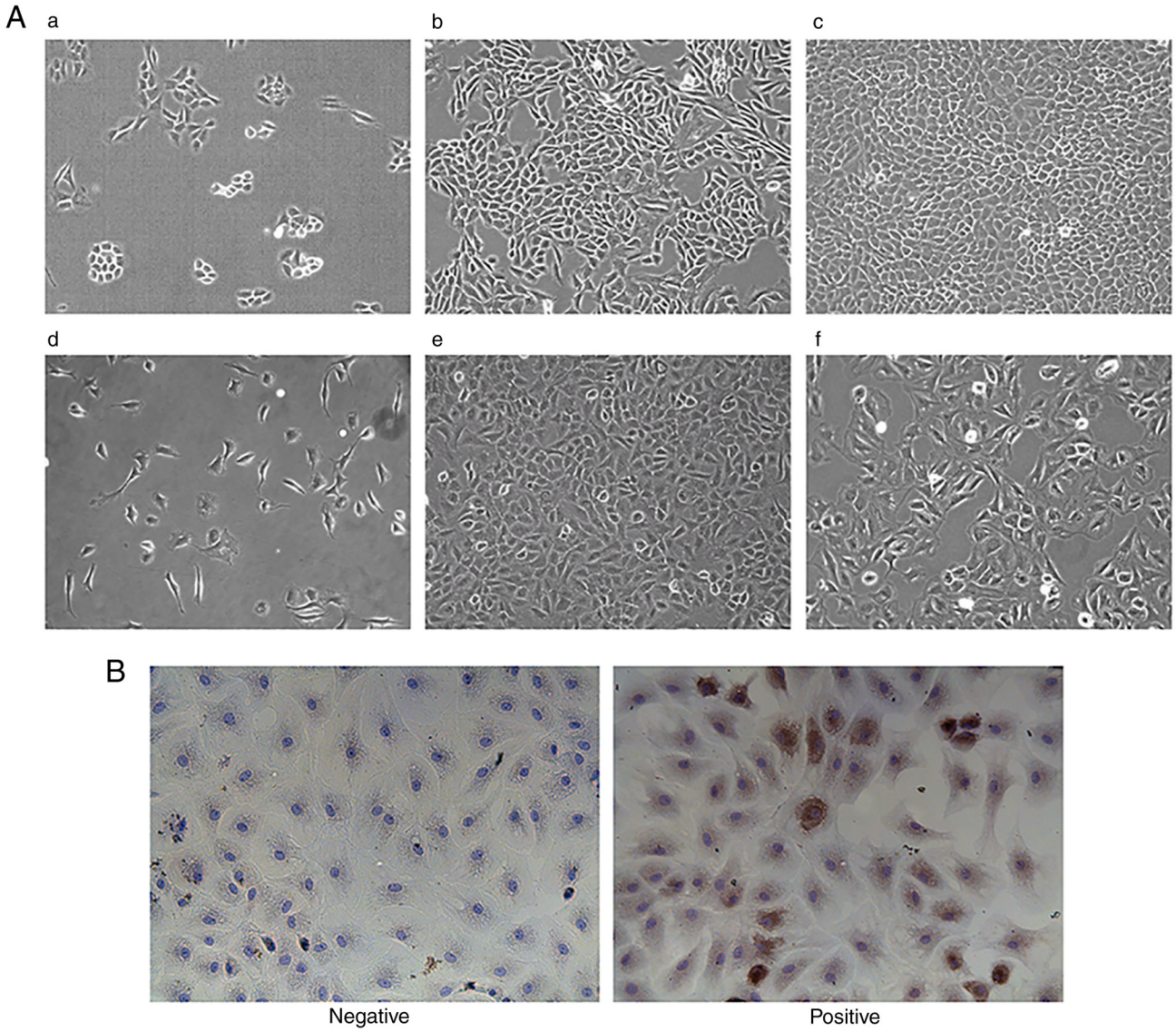

Figure 3. Morphological analysis and characterization of the normal chondrocytes. (A) Morphological changes in the chondrocytes were observed using an inverted phase contrast light microscope. (a) Primary cell culture for day 1; (b) Primary cell culture for day 7; (c) First filial generation cell culture for day 3; (d) Second filial generation cell culture for day 1; (e) Second filial generation cell culture for day 2; (f) Third filial generation cell culture for day 2. Magnification, x100. (B) Immunocytochemical staining for Collagen II. Collagen II in the cytoplasm is stained brownish yellow and the nucleus is stained blue. Magnification, x200.

degraded cells, with overlapping and fuzzy edges, more pseudopods and a slowed rate of proliferation. Therefore, F2 cells were selected for subsequent cell experiments. In Fig. 3B, Collagen II in the extracellular matrix of chondrocytes was stained by immunocytochemistry (DAB method), with the cytoplasm exhibiting a brownish-yellow color and the nucleus exhibiting a blue color. In the negative group, the nucleus exhibited a blue color, while no brownish-yellow color was seen in the cytoplasm. It was concluded that the experimental cells could synthesize Collagen II and proteoglycan, and had the function of chondrocytes, so were given this identification. CCK-8 assay results showed that the inhibition rate of chondrocytes increased with increasing H_2O_2 concentration (Fig. 4A). Similarly, flow cytometry results also showed that the apoptosis rate increased with increasing H_2O_2 concentration (Fig. 4C). Subsequently, using DAPI staining, compared with the control group, the model group treated with 500 μM H_2O_2, in the early stage of apoptosis, exhibited condensation of the nucleus resulting in uneven DAPI staining of the nucleus due to the aggregation of chromatin on the side of the nucleus. In the later stages of apoptosis, the nucleus of the apoptotic cell exhibited round vesicles of different sizes, which were likely apoptotic vesicles (Fig. 4B). Western blotting results showed that compared with the control group, the expression of PARP1 in the model group was reduced, and the expression of cleaved PARP1 increased (Fig. 4D-F), which showed that the model of articular chondrocyte apoptosis was successfully established, and it could be used for subsequent experiments.

Effect of PARP1 knockdown on the apoptosis of chondrocytes. The transfection efficiency of all three viruses reached >80% when using HiTransG P transfection enhancement solution and an MOI of 100. The effective transfection conditions for all three PARP1-knockdown lentiviruses included MOI=100,

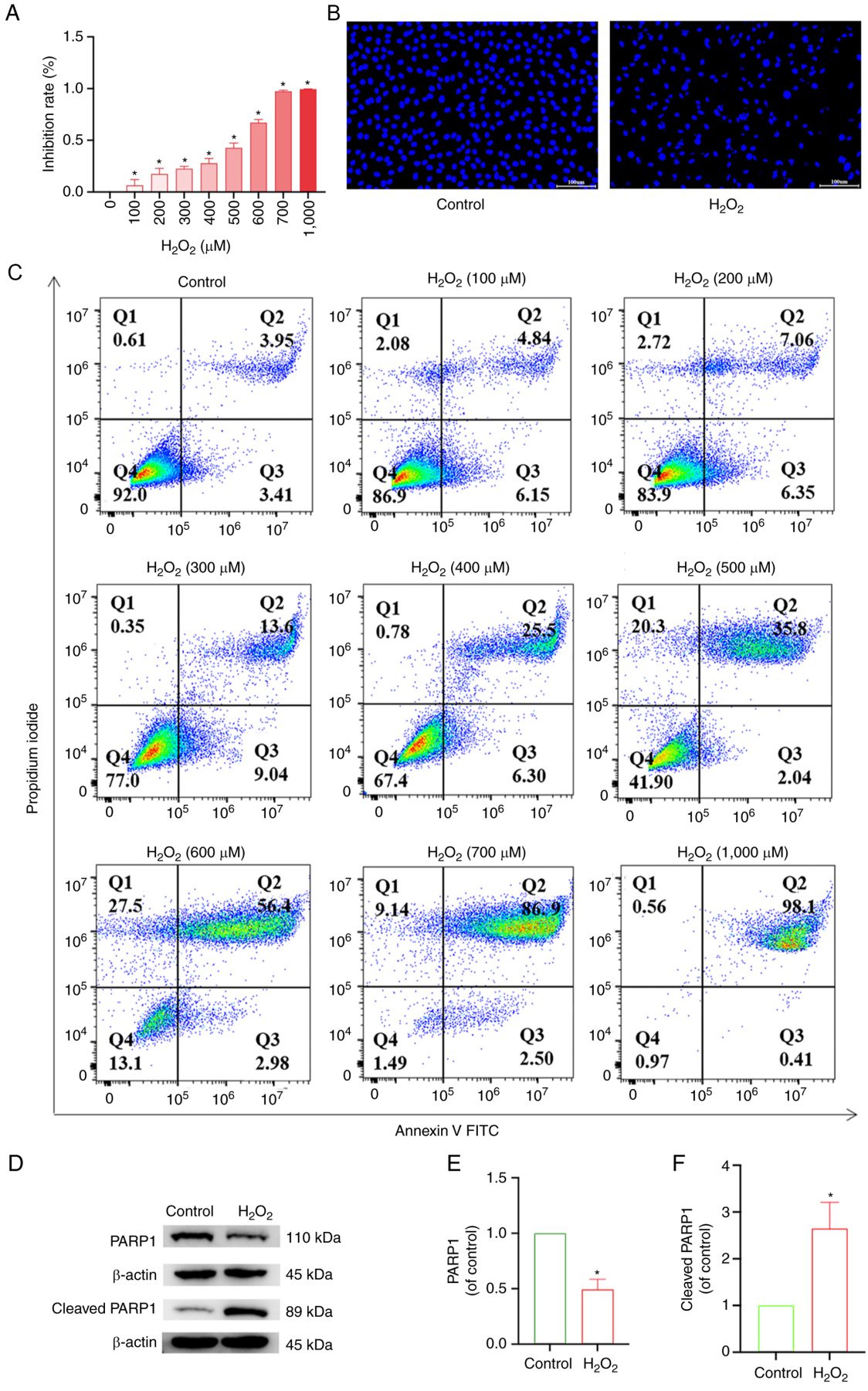

Figure 4. Replication and characterization of the apoptotic articular chondrocyte cell model. (A) Effect of different concentrations of H_2O_2 on the inhibition rate of chondrocytes. (B) DAPI staining identifies apoptosis model. Magnification, x200. (C) Effect of different concentrations of H_2O_2 on the apoptotic rate of chondrocytes. (D) Protein expression levels of PARP1 and cleaved PARP1 in chondrocytes. Quantitative analysis of the relative protein expression levels of (E) PARP1 and (F) cleaved PARP1. *P<0.05 vs. control group. PARP1, poly [ADP-ribose] polymerase-1; H_2O_2, hydrogen peroxide.

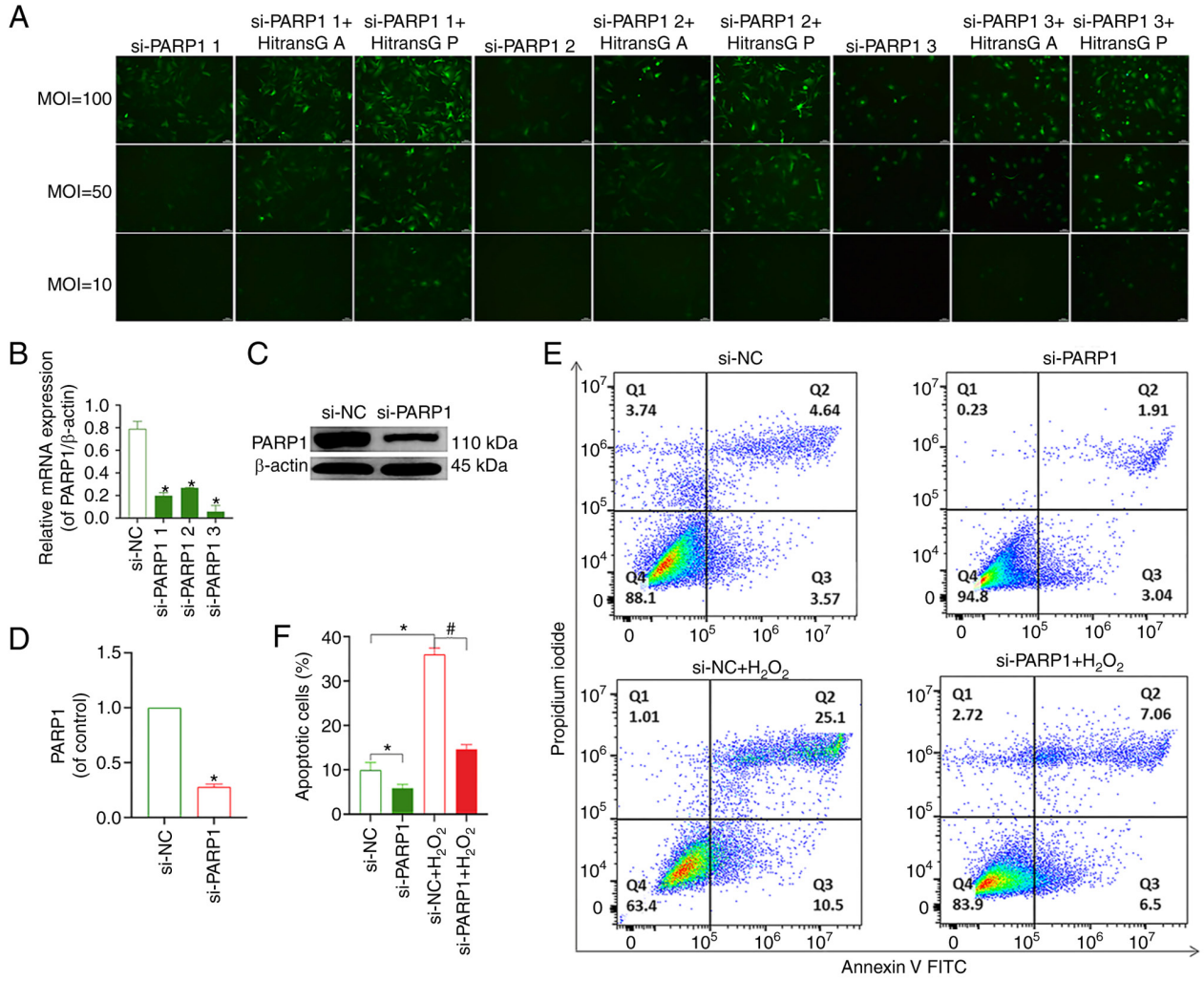

Figure 5. Effect of transfection with a PARP1-knockdown lentivirus on the apoptosis of chondrocytes. (A) eGFP fluorescence intensity under different treatment conditions and transfection with the PARP1-knockdown lentivirus. Magnification, x100. PARP1 (B) mRNA and (C) protein expression levels after transfection with three different PARP1-knockdown lentiviruses. *P<0.05 vs. si-NC group. (D) Quantitative analysis of the relative protein expression levels of PARP1. *P<0.05 vs. si-NC group. (E) Apoptosis of chondrocytes in groups following PARP1 knockdown. (F) Analysis of chondrocyte apoptosis rate in the different groups. *P<0.05 vs. si-NC group; #P<0.05 vs. si-NC+ H_2O_2 group. si, small interfering RNA; NC, negative control; MOI, multiplicity of infection; PARP1, poly [ADP-ribose] polymerase-1; H_2O_2, hydrogen peroxide.

the transfection enhancement reagent was HitransG P and the length of time after which the solution was changed following transfection was 16 h (Fig. 5A). The results of RT-qPCR and western blotting showed that PARP1 expression was lowest in cells transfected with si-PARP1 #3 (Fig. 5B-D); thus, this construct was used for all subsequent experiments. The flow cytometry results showed that chondrocyte apoptosis was decreased in the si-PARP1 group compared with that in the si-NC group. Compared with the si-NC group, the rate of apoptosis was increased in the si-NC+ H_2O_2 group. The chondrocyte apoptosis rate was decreased in the si-PARP1+ H_2O_2 group compared with the si-NC+ H_2O_2 group (Fig. 5E and F). Meanwhile, it was found that knockdown of PARP1 resulted in a decrease in PARP1, cleaved PARP1, PAR and nucleus AIF and MIF levels, and an increase in cytoplasmic AIF and MIF expression (P<0.05; Fig. 6A-I). In conclusion, the knockdown of PARP1 effectively inhibited chondrocyte apoptosis.

Effect of PJ34-mediated inhibition of PARP1 on chondrocyte apoptosis. Apoptosis is closely related to the target PARP1, and although PJ34 is a commonly used PARP1 inhibitor, its inhibitory effect on chondrocytes is unknown. To determine the cytotoxic effect of PJ34, chondrocytes were exposed to PJ34 at different concentrations (0, 0.001, 0.01, 0.1, 1, 10, 100 and 1,000 μM) for 4.5 h. PJ34 had no effect on the activity of chondrocytes at all tested concentrations (Fig. 7A). Based on a previous study (12), 10 μM PJ34 was selected for subsequent experiments. Moreover, apoptosis was reduced when cells were pretreated with PJ34 hydrochloride, suggesting the PARP1-dependent pathway played a pivotal role in chondrocyte apoptosis (Fig. 7B and C). To understand the mechanism of action and determine the impact of PJ34 on chondrocytes, an immunoblot profiling of key factors was performed. Compared with the model group, the protein expression levels of PAR and nucleus AIF and MIF were downregulated, while that of cytoplasmic AIF and MIF was upregulated in the inhibitor group (P<0.05), and the differences in the protein expression levels of caspase-3, cleaved caspase-3, PARP1, and cleaved PARP1 were not statistically significant. The results of Co-IP suggested that AIF interacted with MIF, and that this

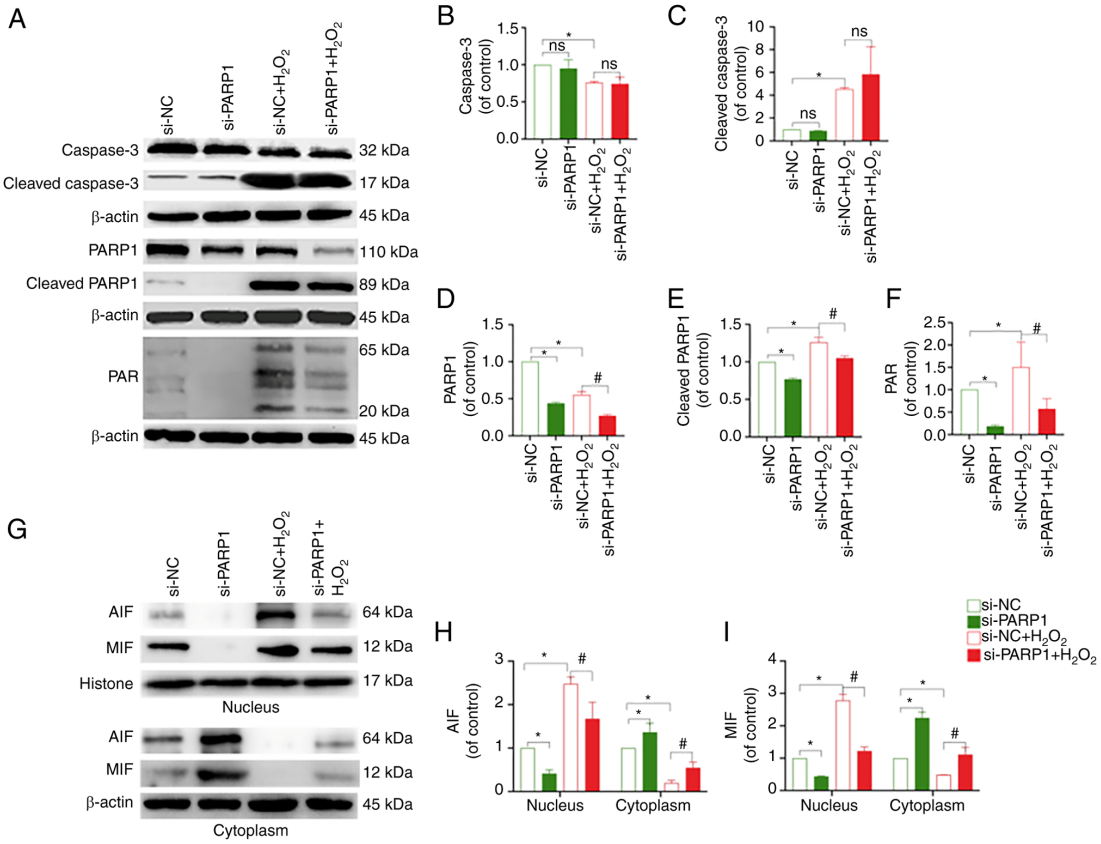

Figure 6. Effect of PARP1 knockdown on the expression of PARP1/AIF pathway-related proteins. (A) Protein expression levels of caspase-3, cleaved caspase-3, PARP1, cleaved PARP1 and PAR in the chondrocytes in the different treatment groups. Quantitative analysis of the relative protein expression levels of (B) caspase-3, (C) cleaved caspase-3, (D) PARP1, (E) cleaved PARP1 and (F) PAR. *P<0.05 vs. si-NC group; #P<0.05 vs. si-NC + H_2O_2 group. (G) Protein expression of AIF and MIF in the nucleus and cytoplasm of chondrocytes in the different treatment groups. Quantitative analysis of the relative protein expression levels of (H) AIF and (I) MIF. *P<0.05 vs. si-NC group; #P<0.05 vs. si-NC + H_2O_2 group. PARP1, poly [ADP-ribose] polymerase-1; PAR, poly ADP-ribose; AIF, apoptosis inducing factor; MIF, migration inhibitory factor; ns, not significant; si, small interfering RNA; NC, negative control; H_2O_2, hydrogen peroxide.

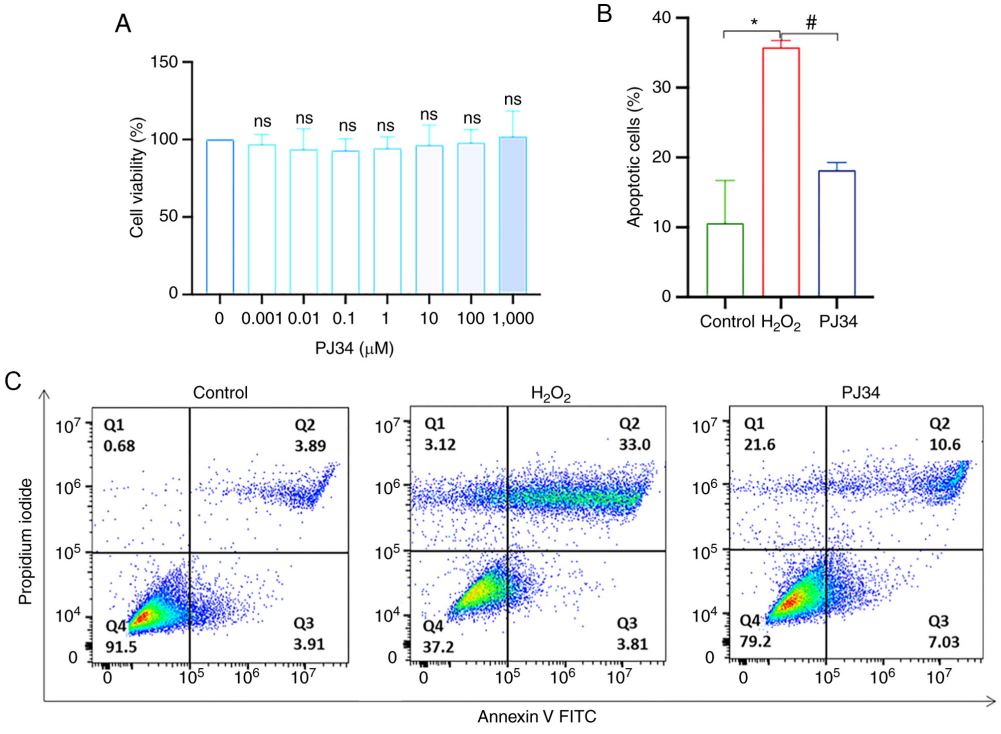

Figure 7. Effect of PJ34-mediated PARP1 inhibition on chondrocyte apoptosis. (A) Effect of different concentrations of PJ34 on chondrocyte activity. (B) Analysis of the chondrocyte apoptosis rates in the different groups. *P<0.05 vs. control group, #P<0.05 vs. H_2O_2 group. (C) Chondrocyte apoptosis rates in the different treatment groups. Ns, not significant; H_2O_2, hydrogen peroxide; PARP1, poly [ADP-ribose] polymerase-1.

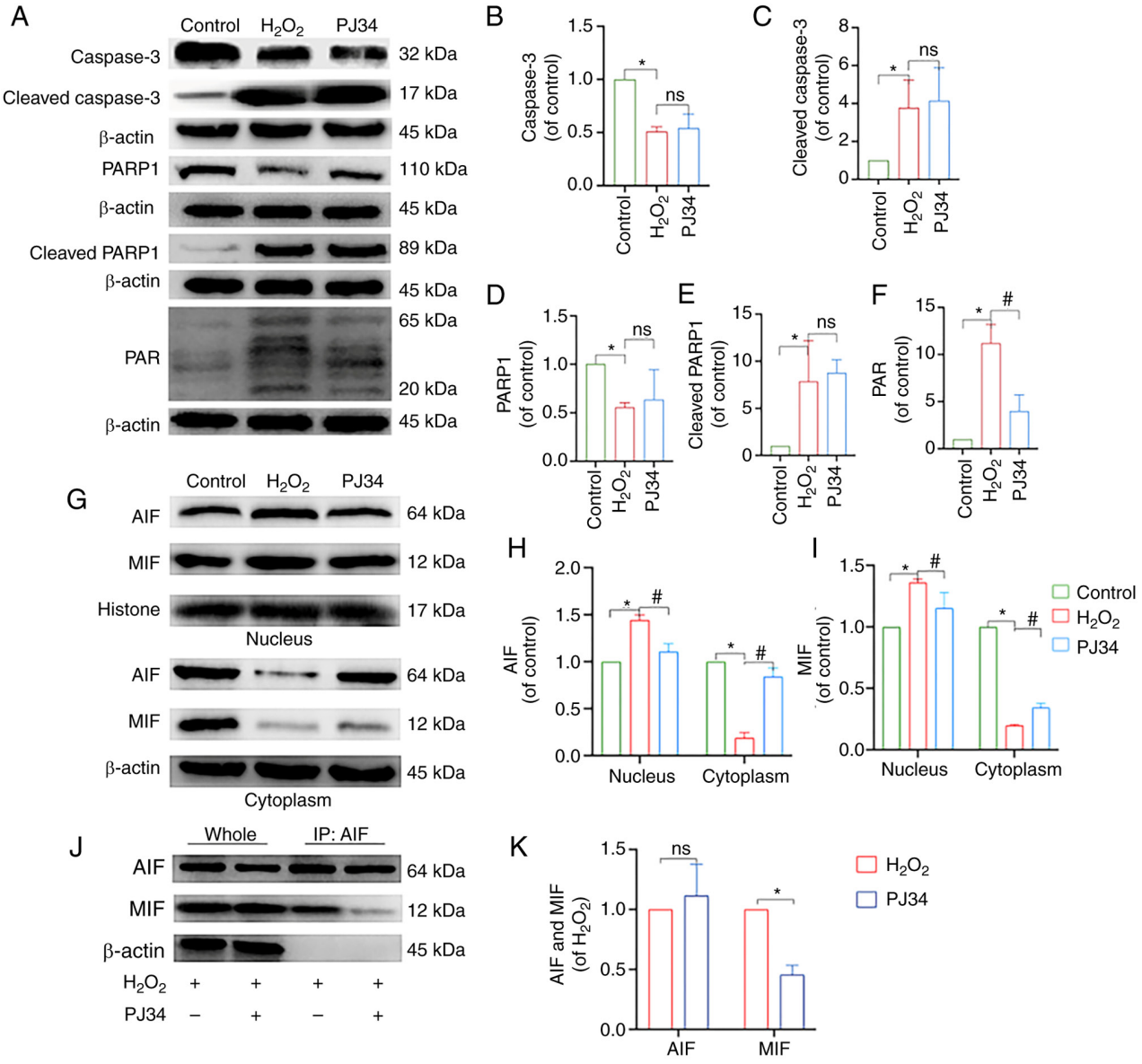

Figure 8. Effect of PJ34-mediated PARP1 inhibition on the expression of PARP1/AIF pathway-related proteins. (A) Protein expression levels of caspase-3, cleaved caspase-3, PARP1, cleaved PARP1 and PAR in chondrocytes in each treatment group. Quantitative analysis of the relative protein expression levels of (B) caspase-3, (C) cleaved caspase-3 (D) PARP1, (E) cleaved PARP1 and (F) PAR. (G) Protein expression levels of AIF and MIF in the nucleus and cytoplasm of the chondrocytes in the different treatment groups. Quantitative analysis of the relative protein expression levels of (H) AIF and (I) MIF. (J) IP analysis of AIF with MIF, where the immunoprecipitate is AIF. (K) Analysis of AIF and MIF protein interactions. *P<0.05 vs. control group; #P<0.05 vs. H_2O_2 group. PARP1, poly [ADP-ribose] polymerase-1; PAR, poly ADP-ribose; AIF, apoptosis inducing factor; MIF, migration inhibitory factor; H_2O_2, hydrogen peroxide; ns, not significant; IP, immunoprecipitation.

interaction was reduced by the addition of PJ34. In summary, inhibition of PARP1 effectively reduced chondrocyte apoptosis (Fig. 8A-K).

RJNTF inhibits chondrocyte apoptosis by regulating the PARP1/AIF pathway. As it was aforementioned, chondrocyte apoptosis was at least partly mediated by the PARP1/AIF pathway. Using CCK-8 assays, 800, 1,600 and 3,200 μg/ml RJNTF were finally selected to treat cells for 48 h for the subsequent experiments (Fig. 9A). The flow cytometry results showed that compared with the model group, the apoptotic rate of chondrocytes was reduced in the RJNTF low, medium and high dose group, and the apoptotic rate of chondrocytes in the RJNTF high dose group was lower in the PJ34 treated group (P<0.05; Fig. 9B and C). Western blotting showed that compared with the model group, the protein expression levels of cleaved caspase-3, cleaved PARP1, PAR, and nucleus AIF and MIF were downregulated, and PARP1, caspase-3, and cytoplasmic AIF and MIF were upregulated in the RJNTF medium and high dose groups (P<0.05). Compared with the inhibitor group, caspase-3 and PARP1 protein expression levels were upregulated in the RJNTF high dose groups, and cleaved caspase-3, cleaved PARP1 and protein expression levels were downregulated in the RJNTF high dose groups (P<0.05; Fig. 10A-F). AIF and MIF protein expression levels were detected in the precipitates of both the model group and the RJNTF group, indicating that there was an interaction between AIF and MIF, and this interaction was reduced after

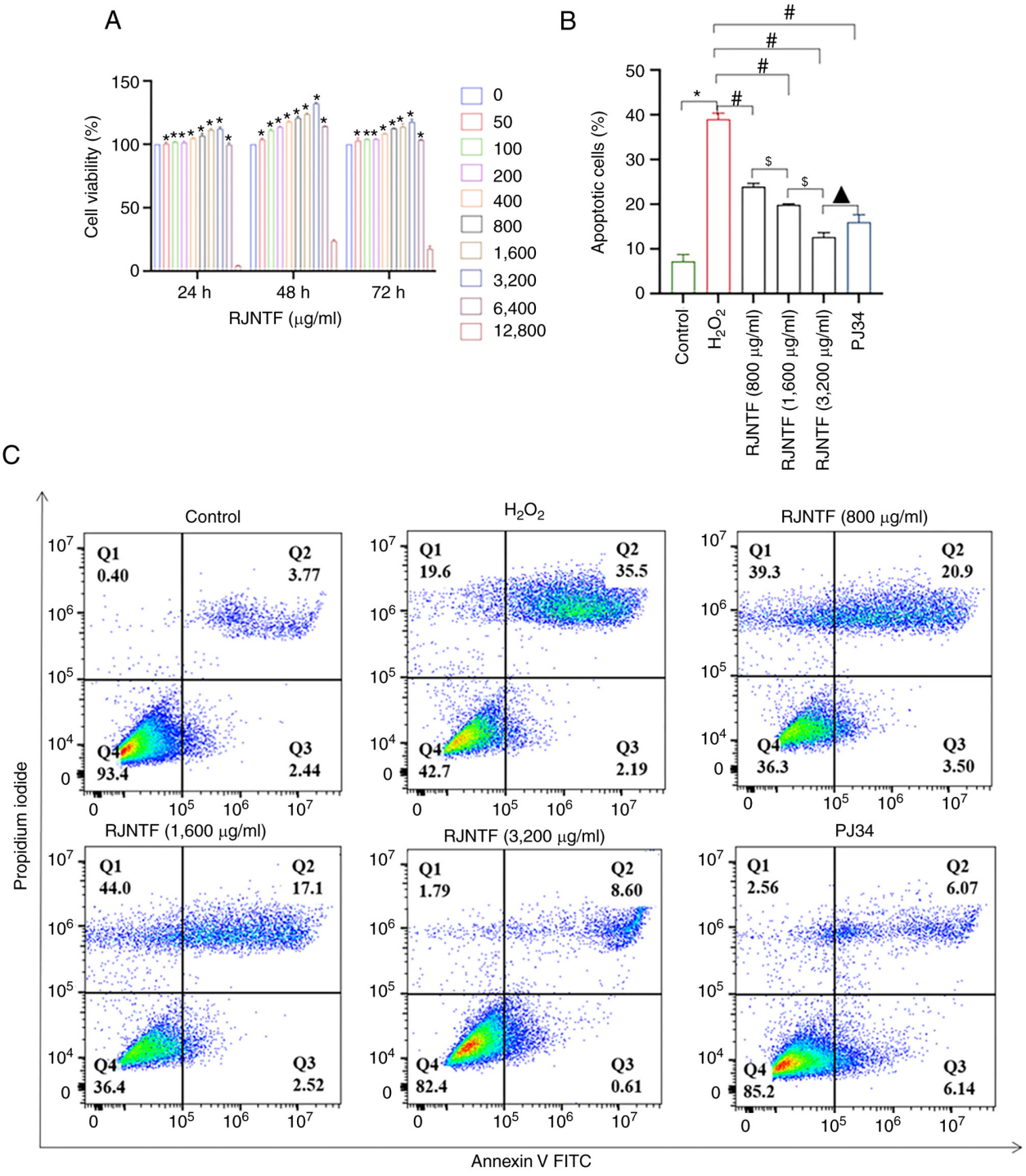

Figure 9. RJNTF inhibits chondrocyte apoptosis by regulating the PARP1/AIF pathway. (A) Chondrocytes were incubated for with different concentrations of RJNTF for 24, 48, or 72 h. Cell viability was assessed using a Cell Counting Kit-8 assay. (B) Analysis of the chondrocyte apoptosis rate in the different groups. (C) Apoptotic rate of chondrocytes in the different groups. *P<0.05 vs. control group; #P<0.05 vs. H_2O_2 group, $P<0.05 vs. RJNTF group, ▲P<0.05 vs. 3,200 μg/ml RJNTF group. PARP1, poly [ADP-ribose] polymerase-1; AIF, apoptosis inducing factor; RJNTF, Rongjin Niantong Fan; H_2O_2, hydrogen peroxide.

the addition of RJNTF (Fig. 11A-E). In conclusion, RJNTF could effectively reduce chondrocyte apoptosis by inhibiting the PARP1/AIF pathway.

Discussion

Network pharmacology analysis of protein interactions showed that RJNTF exerted its beneficial effects on KOA via regulation of STAT3, PI3K, RAF, RAS, AKT, PARP1, JALK2 and PARP1. Sun *et al* (38) found that TANK-binding kinase 1 (TBK1) was expressed at high levels in KOA by constructing an animal model of OA in C57BL/6 J mice. TBK1 activated the JAK/STAT signaling pathway, and knockdown of TBK1 inhibited extracellular matrix degradation. The beneficial effect of TBK1 knockdown was abrogated by transfecting cells with a STAT3 overexpression plasmid. AKT1 is an important

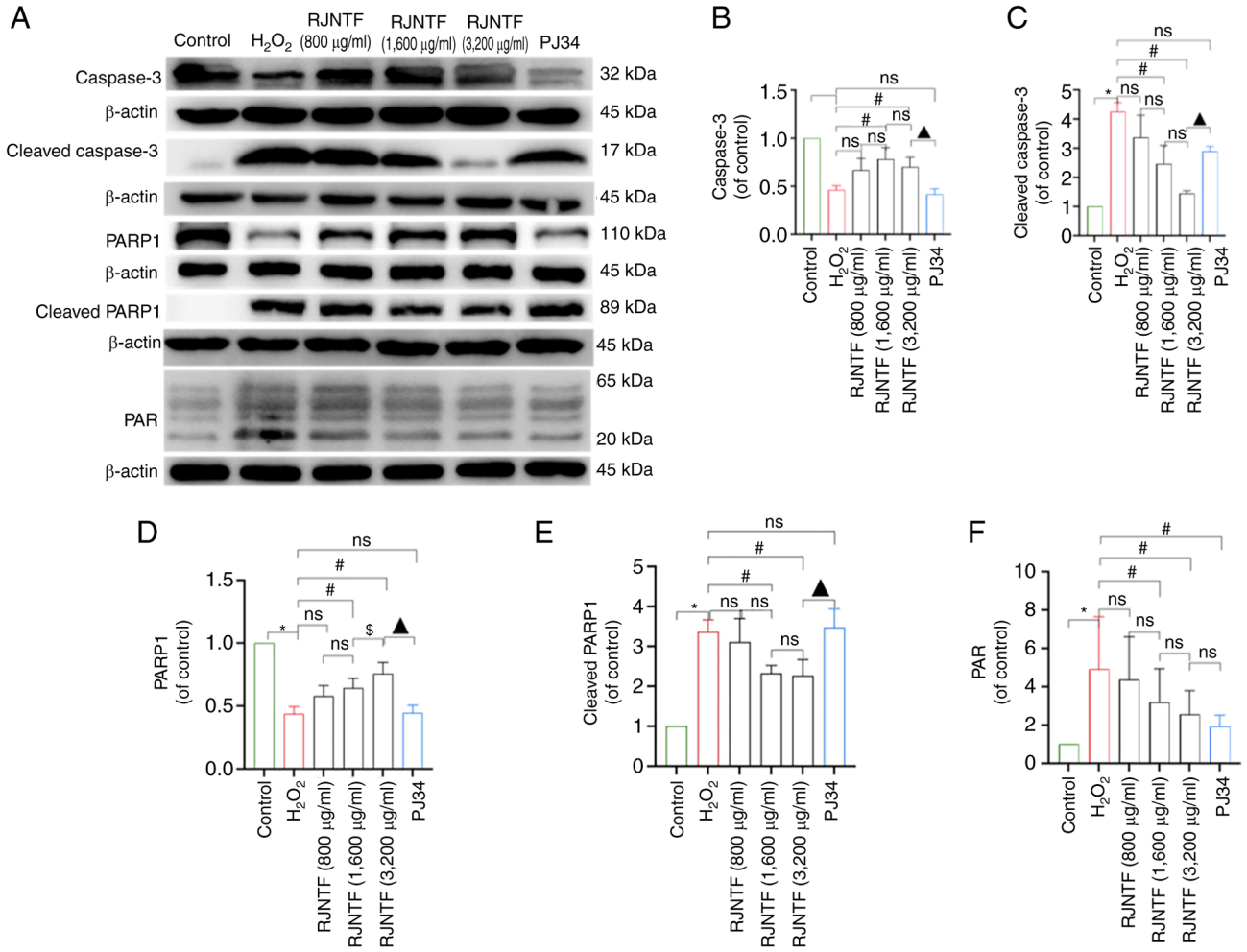

Figure 10. Effect of RJNTF on the expression of PARP1/AIF pathway-related proteins. (A) The protein expression levels of caspase-3, cleaved caspase-3, PARP1, cleaved PARP1, and PAR in the chondrocytes in the different treatment groups were determined. Quantitative analysis of the relative protein expression levels of (B) caspase-3, (C) cleaved caspase-3 (D) PARP1, (E) cleaved PARP1 and (F) PAR. *P<0.05 vs. control group; #P<0.05 vs. H_2O_2 group; $P<0.05 vs. RJNTF group; ▲P<0.05 vs. 3,200 μg/ml RJNTF. PARP1, poly [ADP-ribose] polymerase-1; PAR, poly ADP-ribose; AIF, apoptosis inducing factor; H_2O_2, hydrogen peroxide.

downstream target kinase in the PI3K/AKT signaling pathway, which can regulate the mTOR signaling pathway and other pathways, IL-1β-induced chondrocyte proliferation, and can reduce apoptosis (39). It has been shown that Ras independently inhibits the activation of Erk1/2. This effect is associated with reduced activation of transcription factors such as Elk-1, which inhibits cartilage damage by suppressing major catabolic factors involved in KOA cartilage degradation processes (40). The aforementioned results suggest that the mechanism of KOA action includes proliferation, inflammation and apoptosis (41-44).

KEGG analysis showed that RJNTF exerts its effects on KOA by interfering with multiple signaling pathways such as the NF-κB pathway, apoptotic pathways, the HIF-1 signaling pathway, the JAT-STAT signaling pathway, the IL-17 signaling pathway and other signaling pathways to treat knee joints (45-48). NF-κB is closely related to inflammation, and network pharmacology combined with *in vitro* experiments confirmed that the mechanism of action of Fengshi Gutong Capsule in treating KOA was associated with the NF-κB signaling pathway (49). It has been noted that maintaining a hypoxic environment in the subchondral bone alleviates osteoarthritis progression. HIFs are core regulators that induce hypoxia genes, repair the cellular oxygen environment and play an important role in the treatment of OA (50,51). It has been shown that the IL-17 signaling pathway is highly regulated in synovial tissues of patients with KOA, suggesting that the IL-17 signaling pathway has a better transcriptional response in KOA chondrocytes and synovial tissues, which can induce osteoclastogenesis and bone erosion in arthritic diseases; therefore, the IL-17 signaling pathway may be a potential target gene for the treatment and diagnosis of KOA (52,53). Several pathways play a regulatory role in KOA; among them, PARP1 is closely related to apoptosis (37,54). For example, chaperone-mediated autophagy can inhibit cardiomyocyte apoptosis induced by oxidative stress by inhibiting cleaved PARP1 protein expression (55); aurora kinase A knockdown promotes apoptosis in Epstein-Barr virus-infected atypical glandular cells through cleavage of caspase-3 and -9, and PARP1 (56). Additionally, the colocalization of PARP-1/AIF in the nucleus indicates that PARP-1 plays a pivotal role in AIF-mediated carbon ion pro-apoptosis (14). Therefore, it is hypothesized that RJNTF may exert an inhibitory effect on chondrocyte apoptosis through regulation of the PARP1/AIF

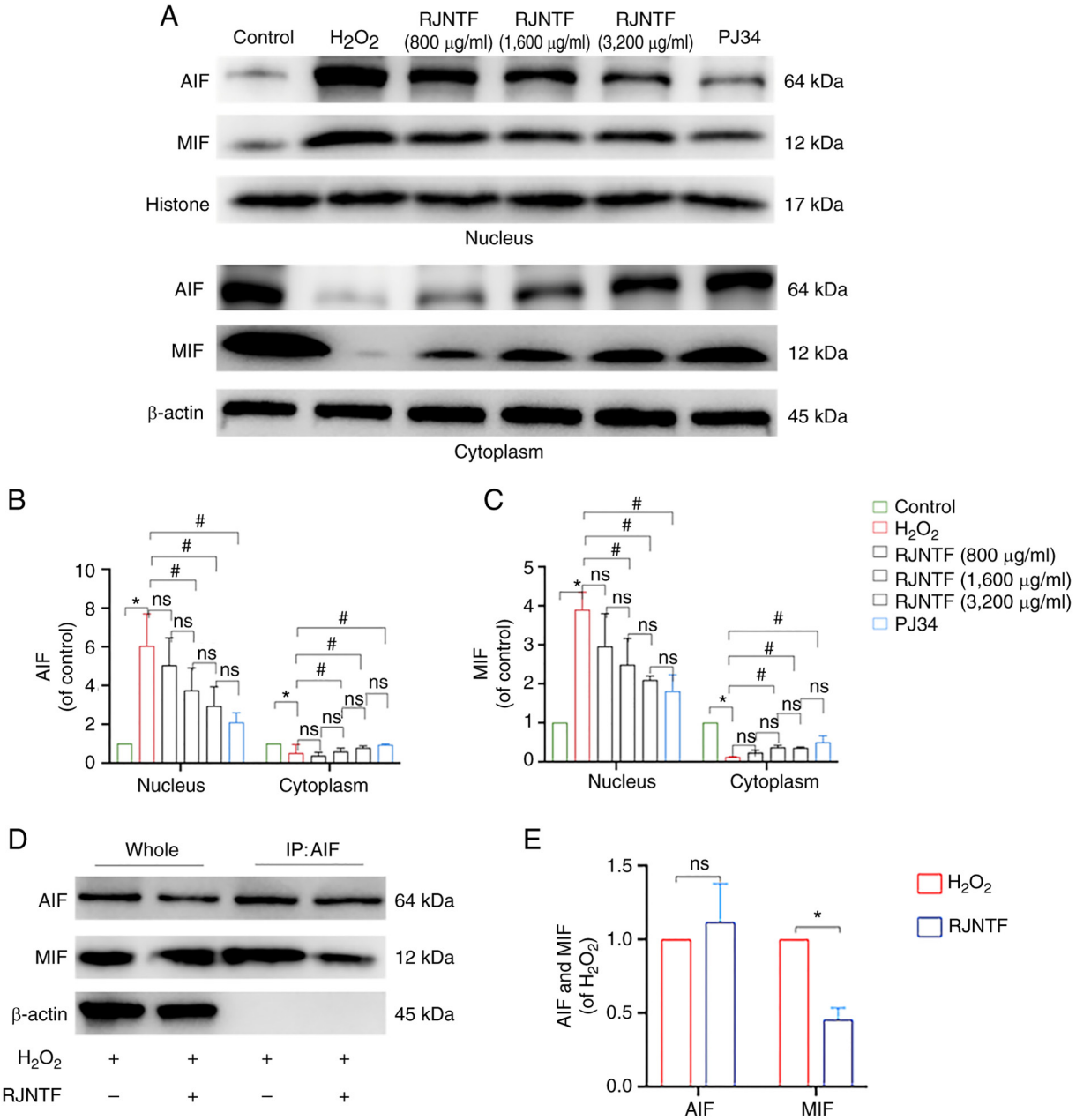

Figure 11. Effect of RJNTF on the expression of PARP1/AIF pathway-related proteins. (A) Expression of AIF and MIF in the nucleus and cytoplasm of chondrocytes in each group. Quantitative analysis of the relative protein expression levels of (B) AIF and (C) MIF. *P<0.05 vs. control group; #P<0.05 vs. H_2O_2 group. (D) Immunoprecipitation analysis of AIF with MIF, where the IP is AIF. (E) Analysis of AIF and MIF protein interactions. *P<0.05 vs. H_2O_2 group. PARP1, poly [ADP-ribose] polymerase-1; AIF, apoptosis inducing factor; MIF, migration inhibitory factor; IP, immunoprecipitate; H_2O_2, hydrogen peroxide; ns, not significant.

pathway, and the subsequent experiments were designed to test this hypothesis.

PARP1 is a DNA repair enzyme expressed in most eukaryotic cells, activated by recognizing structurally damaged DNA fragments and is considered to be a DNA damage, and is also a cleavage substrate for the apoptotic core member protein caspase (57). The primary function of PARP1 is to sense and repair DNA breaks (48). PARP1 binds to DNA strand breaks and then transfers PAR multimers to PARP1 itself, which recruits the DNA repair machinery to DNA damage. PARP1 catalyzes the formation of PAR on histones, which allows it to induce chromatin relaxation in chromatin to increase the viability of the DNA repair machinery to DNA breaks. Thus, PARP1 is activated by activated caspase-3 to inhibit these processes and activate apoptosis when the extent of damage is too large. In the present study, it was found that in chondrocytes, after PARP1-bound DNA strand breaks, activated caspase-3 can cleave PARP1, and the 89-kDa PARP1 fragment is released from the damaged DNA as it can no longer bind the 24-kDa PARP1 fragment to DNA. At the same time, initiation of PAR synthesis results in the release of AIF, translocation to the nucleus in combination with macrophage MIF, and the action of DNA endonuclease and nucleic acid exonuclease G results in chromatin condensation as well as DNA breakage (36). It was found that this type of apoptosis could be inhibited by the PARP1 inhibitor PJ34, but the protein

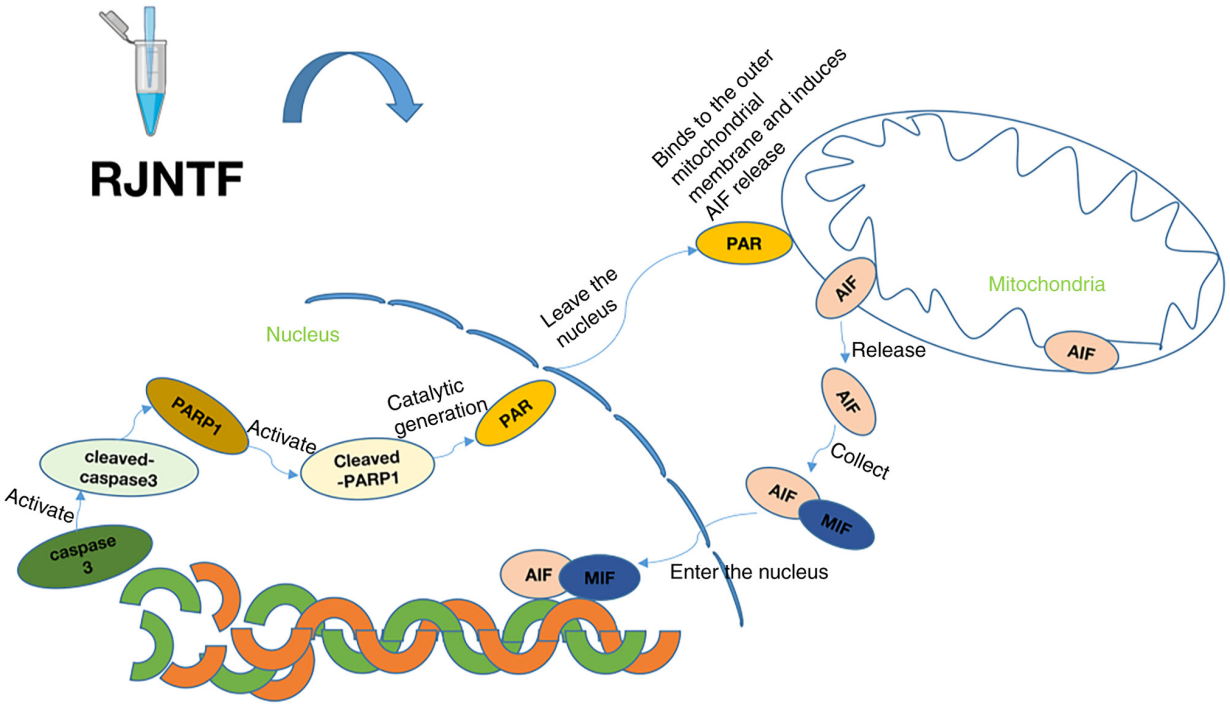

Figure 12. Potential mechanism of action of RJNTF against chondrocyte apoptosis. RJNTF inhibited H_2O_2-induced chondrocyte apoptosis by suppressing the PARP1/AIF signaling pathway. RJNTF, Rongjin Niantong Fang; PARP1, poly [ADP-ribose] polymerase-1; AIF, apoptosis inducing factor; MIF, migration inhibitory factor; PAR, poly [ADP-ribose].

expression levels of PARP1 and cleaved PARP1 were not altered after the addition of PJ34, while PAR expression was notably downregulated, and the phenomenon of AIF and MIF nuclear translocation had been suppressed. Thus, PJ34 further inhibited apoptosis caused by AIF entry into the nucleus by inhibiting the synthesis of PAR.

The flow cytometry results indicated that RJNTF could inhibit chondrocyte apoptosis by interfering with the PARP1/AIF pathway. However, with the addition of RJNTF, although the expression of cleaved caspase-3, cleaved PARP1 and nucleus AIF and MIF decreased and that of caspase-3, PARP1 and cytoplasmic AIF and MIF increased, it did not show a dose-dependent effect with increasing concentrations of RJNTF. Combining the results of flow cytometry, the apoptosis rate of the RJNTF high dose group was lower than that of the PJ34 group; a significant difference which suggests that the use of H_2O_2 modeling not only affected the apoptotic pathway of PARP1/AIF, but also the involvement of other apoptotic pathways. RJNTF can not only inhibit apoptosis by interfering with the PARP1/AIF pathway, but also other pathways to inhibit apoptosis, and thus play a more potent role in inhibiting apoptosis compared with a single inhibitor. Once again, this provides a reliable experimental basis for the multi-targeting and multi-pathway effect of RJNTF in the treatment of KOA.

In conclusion, the present study demonstrated that RJNTF reduces H_2O_2-induced chondrocyte apoptosis via the PARP1/AIF signaling pathway (Fig. 12). These findings highlight novel avenues for understanding the therapeutic mechanism of RJNTF, and provide a reference for further exploration and clinical application of RJNTF. However, it is noteworthy that a limitation of the present study is that it is an *in vitro* study where RJNTF is directly contacted with chondrocytes. This may not reflect the situation *in vivo* since RJNTF is taken orally and is not clear if all the components of RJNTF directly contact the chondrocytes after oral administration; this will be investigated further in future studies.

Acknowledgements

Not applicable.

Funding

The present study was supported by the National Natural Science Foundation of China (grant no. 82074465), the Natural Science Foundation of Fujian Province (grant no. 2022J01843), the Key Laboratory of Integrative Medicine of Fujian Province University (Fujian University of Traditional Chinese Medicine; grant nos. KLIM2022003 and CKJ2022003), the NATCM's Project of High-level Construction of Key TCM Disciplines (Traditional Chinese Orthopedics) (grant no. zyyzdxk-2023106) and the Traditional Chinese Orthopedics Open subject of FJTCM (grant no. XGS2023004).

Availability of data and materials

The data generated in the present study may be requested from the corresponding author.

Authors' contributions

JC and TZ conducted the majority of the experiments. YD and ZC assisted with the immunofluorescence experiments. CZ and

XC performed the flow cytometry. RW and QL performed the statistical analysis, and wrote, reviewed and edited the original manuscript. JC and TZ revised the manuscript. JC, TZ, QL and RW designed the study. GW conceived and designed the study, and wrote, reviewed and edited the original manuscript. RW, YD and GW confirm the authenticity of all the raw data. All authors have read and approved the final version of the manuscript.

Ethics approval and consent to participate

All animals received humane care and the experimental methods were approved by the Animal Care and Use Committee of Fujian University of Traditional Chinese Medicine (Fuzhou, China; approval no. FJTCM IACUC 2022044).

Patient consent for publication

Not applicable.

Competing interests

The authors declare that they have no competing interests.

References

1. Ramírez-Noguera P, Marín IZ, Chavarin BM, Valderrama ME, López-Barrera LD and Díaz-Torres R: Study of the early effects of chitosan nanoparticles with glutathione in rats with osteoarthrosis. Pharmaceutics 15: 2172, 2023.
2. Rousseau JC, Sornay-Rendu E, Bertholon C, Garnero P and Chapurlat R: Serum periostin is associated with prevalent knee osteoarthritis and disease incidence/progression in women: The OFELY study. Osteoarthritis Cartilage 23: 1736-1742, 2015.
3. GBD 2015 Disease and Injury Incidence and Prevalence Collaborators: Global, regional, and national incidence, prevalence, and years lived with disability for 310 diseases and injuries, 1990-2015: A systematic analysis for the global burden of disease study 2015. Lancet 388: 1545-1602, 2016.
4. Yu D, Peat G, Bedson J and Jordan KP: Annual consultation incidence of osteoarthritis estimated from population-based health care data in England. Rheumatology (Oxford) 54: 2051-2060, 2015.
5. Rewald S, Lenssen AFT, Emans PJ, de Bie RA, van Breukelen G and Mesters I: Aquatic cycling improves knee pain and physical functioning in patients with knee osteoarthritis: A randomized controlled trial. Arch Phys Med Rehabil 101: 1288-1295, 2020.
6. Mahmoudian A, Lohmander LS, Mobasheri A, Englund M and Luyten FP: Early-stage symptomatic osteoarthritis of the knee-time for action. Nat Rev Rheumatol 17: 621-632, 2021.
7. Godziuk K, Prado CM, Woodhouse LJ and Forhan M: The impact of sarcopenic obesity on knee and hip osteoarthritis: A scoping review. BMC Musculoskelet Disord 19: 271, 2018.
8. Fang G, Wen X, Jiang Z, Du X, Liu R, Zhang C, Huang G, Liao W and Zhang Z: FUNDC1/PFKP-mediated mitophagy induced by KD025 ameliorates cartilage degeneration in osteoarthritis. Mol Ther 31: 3594-3612, 2023.
9. Song J, Kim EH, Yang JH, Kim D, Robby AI, Kim SA, Park SY, Ryu JH and Jin EJ: Upregulated FOXM1 stimulates chondrocyte senescence in Acot12-/-Nudt7-/- double knockout mice. Theranostics 13: 5207-5222, 2023.
10. Chen C, Yin P, Hu S, Sun X and Li B: Circular RNA-9119 protects IL-1β-treated chondrocytes from apoptosis in an osteoarthritis cell model by intercepting the microRNA-26a/PTEN axis. Life Sci 1: 117924, 2020.
11. Huang P, Chen G, Jin W, Mao K, Wan H and He Y: Molecular mechanisms of parthanatos and its role in diverse diseases. Int J Mol Sci 23: 7292, 2022.
12. Mashimo M, Onishi M, Uno A, Tanimichi A, Nobeyama A, Mori M, Yamada S, Negi S, Bu X, Kato J, *et al*: The 89-kDa PARP1 cleavage fragment serves as a cytoplasmic PAR carrier to induce AIF-mediated apoptosis. J Biol Chem 296: 100046, 2021.
13. Koehler RC, Dawson VL and Dawson TM: Targeting parthanatos in ischemic stroke. Front Neurol 12: 662034, 2021.
14. Xu X, Sun B and Zhao C: Poly (ADP-Ribose) polymerase 1 and parthanatos in neurological diseases: From pathogenesis to therapeutic opportunities. Neurobiol Dis 15: 106314, 2023.
15. Zhang Y, Yang X, Ge X and Zhang F: Puerarin attenuates neurological deficits via Bcl-2/Bax/cleaved caspase-3 and Sirt3/SOD2 apoptotic pathways in subarachnoid hemorrhage mice. Biomed Pharmacother 109: 726-733, 2019.
16. Wang Q, Zhou X, Yang L, Zhao Y, Chew Z, Xiao J, Liu C, Zheng X, Zheng Y, Shi Q, *et al*: The natural compound notopterol binds and targets JAK2/3 to ameliorate inflammation and arthritis. Cell Rep 32: 108158, 2020.
17. Zada S, Pham TM, Hwang JS, Ahmed M, Lai TH, Elashkar O, Kim JH, Kim DH and Kim DR: Chlorogenic acid protects human chondrocyte C28/I2 cells from oxidative stress-induced cell death through activation of autophagy. Life Sci 285: 119968, 2021.
18. Jia C, Hu F, Lu D, Jin H, Lu H, Xue E and Wu D: Formononetin inhibits IL-1β-induced inflammation in human chondrocytes and slows the progression of osteoarthritis in rat model via the regulation of PTEN/AKT/NF-κB pathway. Int Immunopharmacol 113: 109309, 2022.
19. Comblain F, Dubuc JE, Lambert C, Sanchez C, Lesponne I, Serisier S and Henrotin Y: Identification of targets of a new nutritional mixture for osteoarthritis management composed by curcuminoids extract, hydrolyzed collagen and green tea extract. PLoS One 11: e0156902, 2016.
20. Ritchie ME, Phipson B, Wu D, Hu Y, Law CW, Shi W and Smyth GK: Limma powers differential expression analyses for RNA-sequencing and microarray studies. Nucleic Acids Res 20: e47, 2015.
21. R Core Team (2012) R: A language and environment for statistical computing. R Foundation for Statistical Computing, Vienna, Austria. ISBN 3-900051-07-0, URL http://www.R-project.org/.
22. RStudio Team (2015) RStudio: RStudio, Inc., Boston, MA URL http://www.rstudio.com/.
23. Martin A, Ochagavia ME, Rabasa LC, Miranda J, Fernandez-de-Cossio J and Bringas R: BisoGenet: A new tool for gene network building, visualization and analysis. BMC Bioinformatics 11: 91, 2010.
24. Shannon P, Markiel A, Ozier O, Baliga NS, Wang JT, Ramage D, Amin N, Schwikowski B and Ideker T: Cytoscape: A software environment for integrated models of biomolecular interaction networks. Genome Res 13: 2498-2504, 2003.
25. Kanehisa M: 'Post-genome Informatics', Oxford University Press (2000).
26. Yu G, Wang LG, Han Y and He QY: clusterProfiler: An R package for comparing biological themes among gene clusters. OMICS 16: 284-287, 2012.
27. Chen J, Chen N, Zhang T, Lin J, Huang Y and Wu G: Rongjin Niantong Fang ameliorates cartilage degeneration by regulating the SDF-1/CXCR4-p38MAPK signalling pathway. Pharm Biol 60: 2253-2265, 2022.
28. Li X, Xu Y, Li H, Jia L, Wang J, Liang S, Cai A, Tan X, Wang L, Wang X, *et al*: Verification of pain-related neuromodulation mechanisms of icariin in knee osteoarthritis. Biomed Pharmacother 144: 112259, 2021.
29. Lin J, Wu G, Chen J, Fu C, Hong X, Li L, Liu X and Wu M: Electroacupuncture inhibits sodium nitroprusside-mediated chondrocyte apoptosis through the mitochondrial pathway. Mol Med Rep 18: 4922-4930, 2018.
30. Livak KJ and Schmittgen TD: Analysis of relative gene expression data using real-time quantitative PCR and the 2(-Delta Delta C(T)) method. Methods 25: 402-408, 2001.
31. Xia GQ, Zhu MP, Li JW and Huang H: An alkaloid from Menispermum dauricum, dauricine mediates Ca influx and inhibits NF-κB pathway to protect chondrocytes from IL-1β-induced inflammation and catabolism. J Ethnopharmacol 321: 117560, 2024.
32. Zhang H, Wang L, Cui J, Wang S, Han Y, Shao H, Wang C, Hu Y, Li X, Zhou Q, *et al*: Maintaining hypoxia environment of subchondral bone alleviates osteoarthritis progression. Sci Adv 9: eabo7868, 2023.
33. Sun C, Peng S, Lv Z, Guo T and Zhang L: Research of STEAP3 interaction with Rab7A and RACK1 to modulate the MAPK and JAK/STAT signaling in osteoarthritis. Int Immunopharmacol 124: 111034, 2023.
34. Xiao J, Zhang P, Cai FL, Luo CG, Pu T, Pan XL and Tian M: IL-17 in osteoarthritis: A narrative review. Open Life Sci 18: 20220747, 2023.

35. Raghavan A and Shah ZA: Withania somnifera improves ischemic stroke outcomes by attenuating PARP1-AIF-mediated caspase-independent apoptosis. Mol Neurobiol 52: 1093-1105, 2015.
36. Wang Z, Qiu Z, Hua S, Yang W, Chen Y, Huang F, Fan Y, Tong L, Xu T, Tong X, *et al*: Nuclear Tkt promotes ischemic heart failure via the cleaved Parp1/Aif axis. Basic Res Cardiol 117: 18, 2022.
37. Abulikemu A, Zhao X, Qi Y, Liu Y, Wang J, Zhou W, Duan H, Li Y, Sun Z and Guo C: Lysosomal impairment-mediated autophagy dysfunction responsible for the vascular endothelial apoptosis caused by silica nanoparticle via ROS/PARP1/AIF signaling pathway. Environ Pollut 304: 119202, 2022.
38. Sun P and Xue Y: Silence of TANK-binding kinase 1 (TBK1) regulates extracellular matrix degradation of chondrocyte in osteoarthritis by janus kinase (JAK)-signal transducer of activators of transcription (STAT) signaling. Bioengineered 13: 1872-1879, 2022.
39. Huang Z, Shi X, Li X, Zhang L, Wu P, Mao J, Xing R, Zhang N and Wang P: Network pharmacology approach to uncover the mechanism governing the effect of simiao powder on knee osteoarthritis. Biomed Res Int 2020: 6971503, 2020.
40. Boileau C, Martel-Pelletier J, Brunet J, Schrier D, Flory C, Boily M and Pelletier JP: PD-0200347, an alpha2delta ligand of the voltage gated calcium channel, inhibits in vivo activation of the Erk1/2 pathway in osteoarthritic chondrocytes: A PKCalpha dependent effect. Ann Rheum Dis 65: 573-580, 2006.
41. Xue JF, Shi ZM, Zou J and Li XL: Inhibition of PI3K/AKT/mTOR signaling pathway promotes autophagy of articular chondrocytes and attenuates inflammatory response in rats with osteoarthritis. Biomed Pharmacother 89: 1252-1261, 2017.
42. Xu K, He Y, Moqbel SAA, Zhou X, Wu L and Bao J: SIRT3 ameliorates osteoarthritis via regulating chondrocyte autophagy and apoptosis through the PI3K/Akt/mTOR pathway. Int J Biol Macromol 175: 351-360, 2021.
43. Chevalley T, Brandi ML, Cashman KD, Cavalier E, Harvey NC, Maggi S, Cooper C, Al-Daghri N, Bock O, Bruyèreet O, *et al*: Role of vitamin D supplementation in the management of musculoskeletal diseases: Update from an European society of clinical and economical aspects of osteoporosis, osteoarthritis and musculoskeletal diseases (ESCEO) working group. Aging Clin Exp Res 34: 2603-2623, 2022.
44. Hou SM, Chen PC, Lin CM, Fang ML, Chi MC and Liu JF: CXCL1 contributes to IL-6 expression in osteoarthritis and rheumatoid arthritis synovial fibroblasts by CXCR2, c-Raf, MAPK, and AP-1 pathway. Arthritis Res Ther 22: 251, 2020.
45. Zhang XA and Kong H: Mechanism of HIFs in osteoarthritis. Front Immunol 14: 1168799, 2023.
46. Bauer C, Moser LB, Kern D, Jeyakumar V and Nehreret S: The combination of glucocorticoids and hyaluronic acid enhances efficacy in IL-1β/IL-17-treated bovine osteochondral grafts compared with individual application. Int J Mol Sci 24: 14388, 2023.
47. Luo P, Zhao T and He H: IL-38-mediated NLRP3/caspase-1 inhibition is a disease-modifying treatment for TMJ inflammation. Ann N Y Acad Sci 1508: 92-104, 2022.
48. Lepetsos P, Papavassiliou KA and Papavassiliou AG: Redox and NF-κB signaling in osteoarthritis. Free Radic Biol Med 132: 90-100, 2019.
49. Sun Y, Liu J, Wang J, He M, Chen X and Chen L: Network pharmacology integrated with experimental validation revealed the mechanism of Fengshi Gutong capsule in the treatment of osteoarthritis. J Ethnopharmacol 319: 117261, 2024.
50. Li X, Mei W, Huang Z, Zhang L, Zhang L, Xu B, Shi X, Xiao Y, Ma Z, Liao T, *et al*: Casticin suppresses monoiodoacetic acid-induced knee osteoarthritis through inhibiting HIF-1α/NLRP3 inflammasome signaling. Int Immunopharmacol 86: 106745, 2020.
51. Zhang H, Wang L, Cui J, Wang S, Han Y, Shao H, Wang C, Hu Y, Li X, Zhou Q, *et al*: Maintaining hypoxia environment of subchondral bone alleviates osteoarthritis progression. Sci Adv 9: eabo7868, 2023.
52. Mimpen JY, Baldwin MJ, Cribbs AP, Philpott M, Carr AJ, Dakin SG and Snelling SJB: Interleukin-17A causes osteoarthritis-like transcriptional changes in human osteoarthritis-derived chondrocytes and synovial fibroblasts in vitro. Front Immunol 12: 676173, 2021.
53. Liu SC, Hsieh HL, Tsai CH, Fong YC, Ko CY, Wu HC, Chang SL, Hsu CJ and Tang CH: CCN2 facilitates IL-17 production and osteoclastogenesis in human osteoarthritis synovial fibroblasts by inhibiting miR-655 expression. J Bone Miner Res 37: 1944-1955, 2022.
54. Alemasova EE and Lavrik OI: Poly (ADP-ribosyl)ation by PARP1: Reaction mechanism and regulatory proteins. Nucleic Acids Res 47: 3811-3827, 2019.
55. Zhang D, Lai W, Liu Y, Wan R and Shen Y: Chaperone-mediated autophagy attenuates H_2O_2-induced cardiomyocyte apoptosis by targeting poly (ADP-ribose) polymerase 1 (PARP1) for lysosomal degradation. Cell Biol Int 46: 1915-1926, 2022.
56. Varshney N, Murmu S, Baral B, Kashyap D, Singh S, Kandpal M, Bhandari V, Chaurasia A, Kumar S and Jha HC: Unraveling the Aurora kinase A and Epstein-Barr nuclear antigen 1 axis in Epstein Barr virus associated gastric cancer. Virology 588: 109901, 2023.
57. Sonar SA, Meitei HT, Karmakar S, Mishra A, Inamdar S, Lenka N and Lal G: Th17 cell promotes apoptosis of IL-23R neurons in experimental autoimmune encephalomyelitis. Clin Immunol 259: 109898, 2024.